Scattering from 3-D Cavities with a Plug and Play Numerical Scheme Combining IE, PDE, and Modal Techniques

André Barka, Paul Soudais, and Dominique Volpert

***Abstract*—In this paper, we present a multidomain and multimethod coupling scheme called FACTOPO, based on generalized scattering matrix computations on three-dimensional (3-D) subdomains. The global target Ω is split in N_V subdomains $(V_i)_{i=1,N_V}$, separated by N_I fictitious surfaces $(\Gamma_j)_{j=1,N_I}$. We use a modal representation of the tangent fields on the interfaces. In each domain, the generalized Scattering matrix S_i is computed with different methods such as the 3-D finite-element method (FEM) or the electric field integral equation (EFIE). This coupling scheme leads to an important reduction in computational resources, especially for cavities with one dimension much larger than the other two. The advantages of this formulation for parametric studies will be illustrated by two cases: computing the RCS of an air-intake terminated with a flat PEC or a fan (CHANNEL) and of an antenna structure coupled to an electronic feed with a varying parameter (DENEB). Numerical as well as experimental results are presented.**

***Index Terms*—Boundary integral equations, cavities, electromagnetic scattering, finite-element method, mode matching.**

I. Introduction

THE electromagnetic scattering from the interior of a complex jet engine inlet contributes significantly to the overall radar cross section (RCS) of a modern jet aircraft. The scattering mechanisms in jet or missile inlets are complicated and difficult to simulate accurately. The geometry is both complicated (engine face, structural obstacles, materials) and electrically large.

In previous work, asymptotic techniques have been employed, such as the geometrical shooting and bouncing ray method (SBR), and hybrid combinations of asymptotic high frequency and modal methods ([1], [2]) to propagate the fields from the inlet opening to the engine face. Hybrid SBR finite-difference time-domain (FDTD), physical optics (PO)-FDTD ([3]) and SBR-modal finite-element method (FEM) ([4]) were presented for analyzing the scattering from three-dimensional (3-D) inlet cavities. In these hybrid methods, the FDTD or the FEM are used to determine the reflection matrices associated with the termination. The modal analysis, PO, or rays are used to analyze the air intake. However, for the channels, these techniques are limited to the high-frequency region. Hybrid numerical methods have been developed in the frequency domain so as to combine both the advantages of the integral equations (IE) for unbounded domains, and the FEM

Manuscript received May 25, 1999; revised October 22, 1999.

The authors are with the Department Electrmagnetisme et Radar, ONERA, BP 72 92322 Châtillon Cedex, France.

Publisher Item Identifier S 0018-926X(00)04373-8.

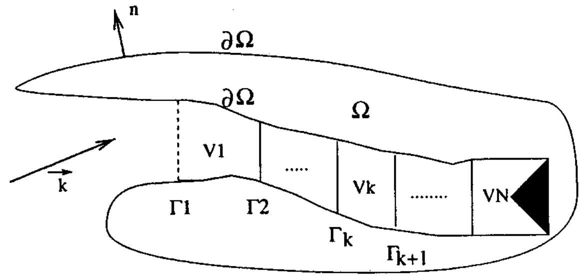

Fig. 1. Target decomposition.

to efficiently model inhomogeneous and anisotropic media ([5]–[11]). They are widely used for the RCS evaluation of large and complex targets, but, unfortunately, many of these formulations are not really suitable in a context of parametric investigations (local inlet engine modifications), or cooperative work during an aircraft project.

Several authors ([7]) have developed connection schemes based on microwave network theory. The 3-D cavity is recessed in an infinite ground plane and is divided into sections and each section is represented by a generalized admittance matrix analyzed independently from the rest of the cavity. Number of formulations are based on the decoupling of the problem in subdomains ([5], [6]) each one characterized by an admittance matrix. In ([7]), the admittance matrix is computed with a boundary-integral method (BIM) and the fields on the interfaces are expanded with local pulse functions. When the cavities are complex, some authors have proposed to compute the admittance matrices with the FEM ([6], [8]).

In this paper, we present a multidomain and multimethod coupling scheme based on generalized scattering matrix computations of 3-D subdomains. The global target Ω is split into N_V subdomains $(V_i)_{i=1,N_V}$ separated by N_I fictitious surfaces $(\Gamma_j)_{j=1,N_I}$ (Fig. 1). We use waveguide modes as expansion functions on the fictitious surfaces for modeling the field propagation from the cavity aperture down to the cavity termination. For each subdomain (even the exterior 3-D volume), the generalized Scattering matrix S_i is computed with different methods such as the 3-D FEM or the electric field integral equation (EFIE) combined with a generalized waveguide modal representation of the fields on the fictitious surfaces ([12], [13]). Then, the different objects are connected by cascading the different S matrices. In a context of parametric investigations, the scattering matrices of the modified domains have to be re-evaluated, the other ones are simply re-used in the connection step. This strategy reduces significantly the computation time compared to traditional hybrid methods for which a geometric or electromagnetic modification requires a new computation of the complete target. Furthermore, the S_i matrix computations are totally independent allowing code and data protection during a multi-industrial aircraft project.

We will emphasize the strong reduction in computational resources obtained with this coupling scheme and especially the waveguide modal expansion. The advantages of this formulation for parametric studies will be illustrated by two cases: computing the RCS of an air intake terminated by a flat PEC or a fan and of an antenna structure coupled to an electronic feed with a varying parameter.

II. Formulation

The target Ω is split into N_V subdomains $(V_i)_{i=1,N_V}$ by N_I fictitious surfaces $(\Gamma_j)_{j=1,N_I}$ (Fig. 1). Note that V_0 is an unbounded volume, and the volumes $\{V_1,\cdots,V_{N_V}\}$ are bounded. In each bounded or unbounded volume V_i of the decomposition, the boundary ∂V_i is made of n_i fictitious surfaces Γ_j and a part of $\partial\Omega$. The surrounding medium has permittivity ε_0 and permeability μ_0. The scatterer is illuminated by an incident wave $\{E_{\text{inc}}, H_{\text{inc}}\}$ with wavenumber $k=\omega/c$. The electromagnetic fields $\boldsymbol{E}$, $\boldsymbol{H}$ are homogenized by expressing the EFIE and FEM formulations with the fields $E=\sqrt{\varepsilon_0}\boldsymbol{E}$ and $H=\sqrt{\mu_0}\boldsymbol{H}$.

A. EFIE

The exterior problem (in the unbounded region V_0) is recast on the surface ∂V_0 by means of the EFIE. The EFIE, written in weak form, is given by

$$\begin{aligned}\frac{j}{4\pi}\iint_{\partial V_0} & k^2G(\Phi.J')-G((\nabla_S.\Phi).(\nabla'_S.J'))\,ds\,ds'\\ &+\frac{k}{2}\int_{\partial V_0}\Phi.(n\times K)\,ds\\ &+\frac{k}{4\pi}\iint_{\partial V_0}(\nabla'G).(\Phi\times K')\,ds\,ds'\\ =k&\int_{\partial V_0}\Phi.E_{\text{sources}}\,ds \qquad (1)\end{aligned}$$

with $J=n\times H, K=E\times n, G(r)=e^{-jkr}/r\,, r=\|\vec{MM'}\|$, the primed quantities (e.g., J') are taken at the emission point M', the others are taken at the observation point M.

The functions Φ are the Rao–Wilton–Glisson (RWG) divergence-conforming basis functions ([14]) used for the discretization of the boundary integral equation.

The linear system is solved with an out-of-core solver with asynchronous I/O. Very efficient out-of-core solvers exist on supercomputers, workstations and PC's. They are very attractive for applications with large number of right hand sides.

B. FEM

The weak form of the partial differential equation for the interior problem in V_i relates the magnetic field in the volume to the trace of the tangential electric field (or equivalently $n\times E$) on its boundary ∂V_i

$$\begin{aligned}j\int_{V_i}k^2(\mu H).\varphi\,dv-j\int_{V_i}(\varepsilon^{-1}\nabla\times H).(\nabla\times\varphi)\,dv\\ =-k\int_{\partial V_i}(n\times E).\varphi\,ds. \qquad (2)\end{aligned}$$

The interior problem 2 is discretized with tetrahedral curl-conforming edge-elements functions φ ([15]). These elements guarantee that the null space of the curl operator is correctly approximated (no spurious modes are added to the solution). With these elements, only the tangential components of the fields are continuous at element boundaries, i.e., the normal components are allowed to jump, which is the correct physical property.

C. Modal Functions on the Fictitious Surfaces

On each fictitious surface Γ_j of V_i, the tangential fields ($n\times E$, $n\times H$) are expanded in a set of waveguide mode functions ($n\times E_p^j$, $n\times H_p^j$). For clarity in the following formulation, the functions $n\times E_p^j$ are extended by zero on all the other surfaces of ∂V_i. These modes are computed on planar surfaces of any shape with a scalar potential formulation ([12]) discretized with an FEM generalized to compute the dispersion characteristics ([13]). If p_j denotes the number of modes on Γ_j, the total tangential fields are written as

$$\begin{cases}(n\times E)_{\Gamma_j}=\sum\limits_{p=1,p_j}(a_{i,p}^j+b_{i,p}^j)(n\times E_p^j)\\ (n\times H)_{\Gamma_j}=\sum\limits_{p=1,p_j}(a_{i,p}^j-b_{i,p}^j)(n\times H_p^j).\end{cases} \qquad (3)$$

If V_i has n_i interfaces, the total number of modes is $\sum_{j=1,n_i}p_j$. We shall now introduce these field decompositions in the EFIE and FEM formulations (1), (2). By linearity of the Maxwell equations, the tangent magnetic field on ∂V_i is a linear combination of the following fields:

$$\begin{aligned}(n\times H)_{\partial V_i}=\sum_{j=1,n_i}\sum_{p=1,p_j}(a_{i,p}^j+b_{i,p}^j)(n\times H_{\text{excitation}}^{j,p})_{\partial V_i}\\ +(n\times H_{\text{source}})_{\partial V_i} \qquad (4)\end{aligned}$$

$n\times H_{\text{excitation}}^{j,p}$ is a tangent magnetic field defined on the surface ∂V_i induced by the pth electrical modal field $n\times E_p^j$ belonging to the interface j and extended by zero on the other surfaces. In the same way, $n\times H_{\text{source}}$ is the tangent magnetic field on ∂V_0 induced by the incident wave $\{E_{\text{inc}}, H_{\text{inc}}\}$ illuminating the scatterer when all the fictitious surfaces are perfectly conductive.

The $H_{\text{excitation}}^{j,p}$ can be computed from the following FEM equation for a bounded volume V_i:

$$\begin{aligned}j\int_{V_i}&k^2\,(\mu H_{\text{excitation}}^{j,p}).\varphi\,dv\\ &-j\int_{.V}(\varepsilon^{-1}\,\nabla\times H_{\text{excitation}}^{j,p}).(\nabla\times\varphi)\,dv\\ &=-k\int_{\Gamma_j}(n\times E^j{}_p).\varphi\,ds. \qquad (5)\end{aligned}$$

The EFIE can be used in this formulation to compute the $H^{j,p}_{\text{excitation}}$ fields for both bounded and unbounded volumes

$$\begin{aligned}\frac{j}{4\pi}\iint_{\partial V_i} & k^2 G(\Phi.(J^j_p)') - G((\nabla_S.\Phi).(\nabla'_S.(J^j_p)'))\,ds\,ds' \\ &= -\frac{k}{2}\int_{\Gamma_j}\Phi.(n\times(K^j{}_p))\,ds \\ &\quad - \frac{k}{4\pi}\iint_{\Gamma_j}(\nabla' G).(\Phi\times(K^j_p))')\,ds\,ds' \end{aligned} \tag{6}$$

with $J^j_p = n \times H^{j,p}_{excitation}$, $K^j_p = E^j_p \times n$.

The scatterer is illuminated by an incident wave $\{E_{\text{inc}}, H_{\text{inc}}\}$ located in the exterior unbounded domain V_0. The $J_{\text{source}} = n \times H_{\text{source}}$ field is solution of the following integral equation:

$$\begin{aligned}\frac{j}{4\pi}\iint_{\partial V_0} & k^2 G(\Phi.J'_{\text{source}}) - G((\nabla_S.\Phi).(\nabla'_S.J'_{\text{source}}))\,ds\,ds' \\ &= k\int_{\partial V_0}\Phi.E_{\text{inc}}\,ds. \end{aligned} \tag{7}$$

D. Scattering Matrices

We shall now characterize the volume V_i by its scattering matrix S_i. On all of the n_i fictitious surfaces Γ_j, the tangential components of the total magnetic fields are written

$$\begin{aligned}\sum_{p=1,\,p_j} & (a^j{}_{i,p} - b^j_{i,p}).(n\times H^j_p) \\ &= (n\times H_{\text{source},\,\partial V})_{/\Gamma_j} \\ &\quad + \left(\sum_{j=1,\,n_i}\sum_{p=1,\,p_j}(a^j_{i,p}+b^j_{i,p}).(n\times H^{j,p}_{\text{excitation}})\right)_{/\Gamma_j}. \end{aligned} \tag{8}$$

We define the Hermitian scalar product of the vectors u, v: $\langle u, v\rangle_{\Gamma_j} = \int_{\Gamma_j} u.v^\star\,ds$. By expressing the b^j_i coefficients associated with the outgoing waves in terms of the a^j_i coefficients associated with the incoming waves on the n_i fictitious surfaces, we obtain the following system:

$$\begin{pmatrix} b^1_i \\ \cdot \\ \cdot \\ b^{n_i}_i \end{pmatrix} = \begin{bmatrix} U^{11}_i & \cdot & \cdot & U^{1n_i}_i \\ \cdot & \cdot & \cdot & \cdot \\ \cdot & \cdot & \cdot & \cdot \\ U^{n_i 1}_i & \cdot & \cdot & U^{n_i n_i}_i \end{bmatrix}^{-1} \cdot\left\{\begin{bmatrix} V^{11}_i & \cdot & \cdot & V^{1n_i}_i \\ \cdot & \cdot & \cdot & \cdot \\ \cdot & \cdot & \cdot & \cdot \\ V^{n_i 1}_i & \cdot & \cdot & V^{n_i n_i}_i \end{bmatrix} . \begin{pmatrix} a^1_i \\ \cdot \\ \cdot \\ a^{n_i}_i \end{pmatrix} + \begin{pmatrix} I^1_i \\ \cdot \\ \cdot \\ I^{n_i}_i \end{pmatrix}\right\} \tag{9}$$

with the matrix and vector elements

$$\begin{aligned} I^j_{i\,[p]} &= -\langle n\times H_{\text{source}}, E^j_p\rangle_{\Gamma_j} \\ &\quad \cdot p_j \times 1 \quad column \quad vector \end{aligned} \tag{10}$$

$$\begin{aligned} U^{jj}_i{}_{[p,q]} &= \langle n\times H^{j,p}_{\text{excitation}}, E^j_q\rangle_{\Gamma_j} \\ &\quad + \langle n\times H^j_p, E^j_q\rangle_{\Gamma_j} \quad p_j\times p_j \quad matrix \end{aligned} \tag{11}$$

and

$$\begin{aligned} U^{kj}_i{}_{[p,q]} &= \langle n\times H^{k,p}_{\text{excitation}}, E^j_q\rangle_{\Gamma_j} \\ &\quad \cdot p_j\times p_k \quad matrix \quad \forall\, k\neq j \end{aligned} \tag{12}$$

$$\begin{aligned} V^{jj}_i{}_{[p,q]} &= -\langle n\times H^{j,p}_{\text{excitation}}, E^j_q\rangle_{\Gamma_j} \\ &\quad + \langle n\times H^j_p, E^j_q\rangle_{\Gamma_j} \quad p_j\times p_j \quad matrix \end{aligned} \tag{13}$$

$$\begin{aligned} V^{kj}_i{}_{[p,q]} &= -\langle n\times H^{k,p}_{\text{excitation}}, E^j_q\rangle_{\Gamma_j} \\ &\quad \cdot p_j\times p_k \quad matrix \quad \forall\, k\neq j. \end{aligned} \tag{14}$$

The scattering matrix of V_i is defined by the $S_i = U_i^{-1}.V_i$ matrix of the right hand side of equation (9). The vector $b_{\text{source}} = U_0^{-1}.I_0$ corresponds to the outgoing waves generated by the H_{source} fields in V_0.

After the scattering matrices $S_1, \cdots, S_{N_V}$ of the cavity domains have been computed, the interior domain is assembled with a standard connection scheme ([16, Appendix 1]) yielding the scattering matrix S_{Int}. Finally, the exterior domain V_0 and the interior V_{Int} are assembled by identification of the outgoing waves on the fictitious surface Γ_1. We get the following linear system:

$$[I_d - S_0 S_{\text{Int}}]\{b^1_0\} = \{b_{\text{source}}\}. \tag{15}$$

Then, once the vector $\{b^1_0\}$ has been determined, the total electromagnetic field is recombined on ∂V_0 for all the incident waves

$$\begin{aligned} n\times H_{\partial V_0} &= (n\times H_{\text{source}})_{\partial V_0} + \sum_{j=1,\,n_0}\sum_{p=1,\,p_0} \\ &\quad \cdot (a^j_{0,p}+b^j_{0,p}).(n\times H^{j,p}_{\text{excitation}})_{\partial V_0} \end{aligned} \tag{16}$$

$$n\times E_{\partial V_0} = \sum_{j=1,\,n_0}\sum_{p=1,\,p_0}(a^j_{0,p}+b^j_{0,p}).(n\times E^j_p). \tag{17}$$

III. Test Cases

A. Air Intake Geometry: "CHANNEL"

The geometry of this case is an evolutive channel enclosed in a circular cylinder. The entry of the channel has an elliptic cross section, the end of the channel has a circular cross section. The object is perfectly conducting. The geometry is presented in Fig. 2.

The wave vector of the incident wave for $\phi = 0$ is directed along $-X$, and the electric field is parallel to Y ($\phi\phi$ polarization) or to Z ($\theta\theta$ polarization).

The location of (y_s, z_s) the center of the waveguide cross section is a function of x

$$y_s = -0.048\,78 + 0.116\,\sin^2\left(\frac{\pi}{2}\,\frac{x}{1.360}\right); \qquad z_s = 0.$$

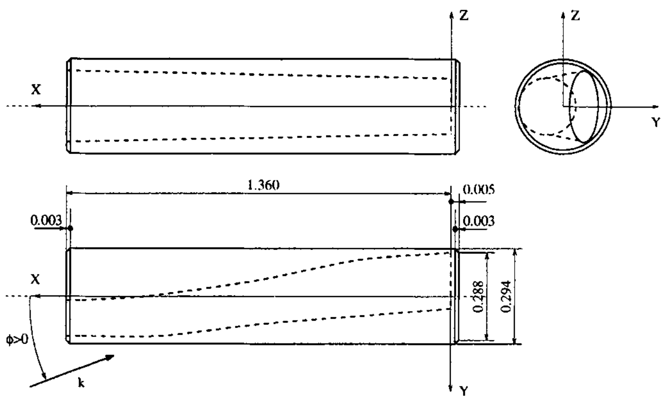

Fig. 2. Geometry of the problem (all dimensions are in meters).

The elliptic cross section is also a function of x

For $0 \leq x \leq 1.300$

$$\left(\frac{z - z_s}{0.118\,03 + 0.025\,68\dfrac{x - 1.300}{1.300}}\right)^2 + \left(\frac{y - y_s}{0.058\,77 - 0.033\,58\dfrac{x - 1.300}{1.300}}\right)^2 = 1.$$

For $1.300 \leq x \leq 1.360$

$$\left(\frac{z - z_s}{0.118\,03}\right)^2 + \left(\frac{y - y_s}{0.058\,77}\right)^2 = 1.$$

The far-field RCS is computed at 2 GHz for the two polarizations $\theta\theta$ and $\phi\phi$ from $-10°$ to 45°. The largest dimension of this case is 9 λ (33 078 unknowns). Next, we introduce a fictitious surface Γ_1 separating V_0 and V_{Int}. Γ_1 is located at 0.075 m from the aperture. In this validation V_0 has been computed with the EFIE (19 353 unknowns) and the interior domain V_{Int} has been evaluated in various different ways. First, V_{Int} has been computed as a single volume and the scattering matrix S_{Int} is computed with the EFIE (13 752 unknowns) or the FEM (87 512 unknowns). In a second step, V_{Int} is split in five domains, each scattering matrix is computed with the EFIE solver and S_{Int} is obtained with the connection algorithm. The tangent fields on the fictitious surface Γ_1 are expanded in seven propagating modes. The two subdomains are assembled by solving a (7×7) linear system of equation (15). Numerical validations of this coupling scheme have been obtained by comparison with a direct EFIE computation of the complete target. The agreement between the direct EFIE and our method is excellent (Figs. 3 and 4).

The second validation is obtained at 3 GHz. We have introduced a spherical incident wave emitted at 8.73 m from the point $(0.592, 0, 0)$ so as to reproduce the measurement conditions (Appendix B). The target is split in two volumes V_0 (39 627 unknowns) and V_{Int} (33 316 unknowns) each one computed with the EFIE. The tangent fields on Γ_1 are expanded with 13 propagating modes. Figs. 5 and 6 show the RCS versus the angle of incidence in the $\phi\phi$ and $\theta\theta$ polarizations. The results are in agreement with the measurements.

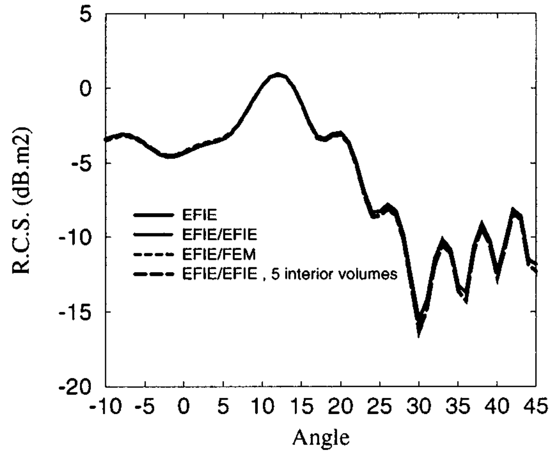

Fig. 3. Comparison of the far-field RCS computed for the air intake, $\phi\phi$ polarization, $F = 2$ GHz.

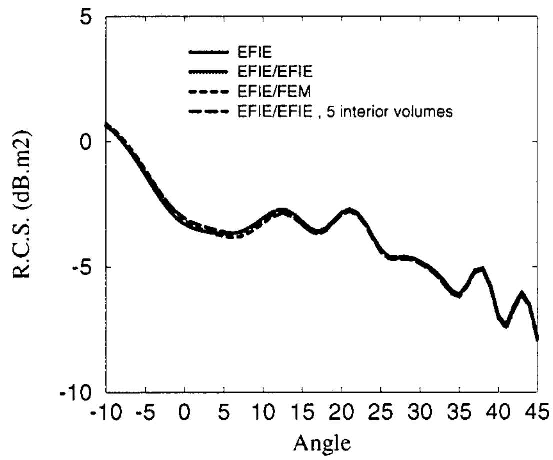

Fig. 4. Comparison of the far-field RCS computed for the air intake, $\theta\theta$ polarization, $F = 2$ GHz.

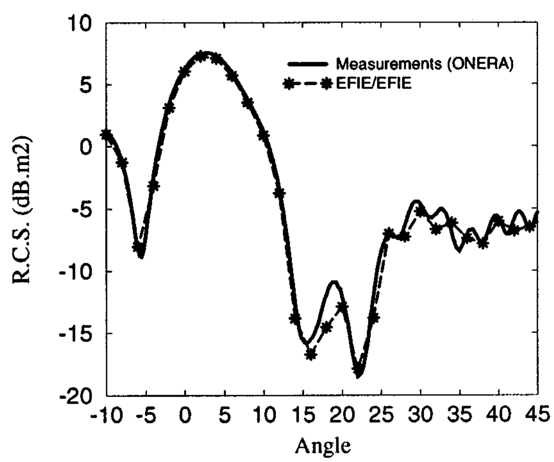

Fig. 5. Comparison of measured and computed near-field RCS for the air intake, $\phi\phi$ polarization, and $F = 3$ GHz.

The third frequency studied is 4 GHz. The largest dimension is 18 λ. A spherical incident wave is again emitted at 8.73 m away from the point (0.592, 0, 0). The mesh of the exte-

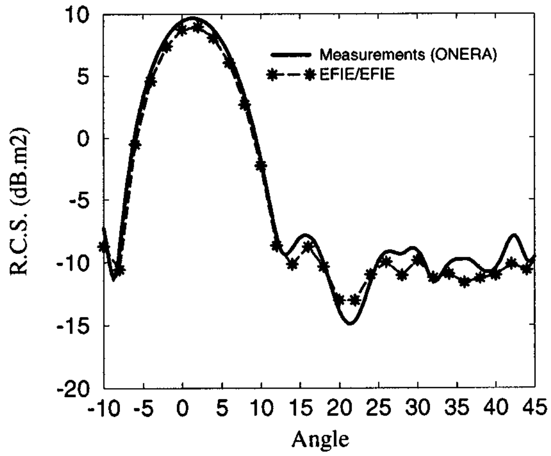

Fig. 6. Comparison of measured and computed near-field RCS for the air intake, $\theta\theta$ polarization, and $F = 3$ GHz.

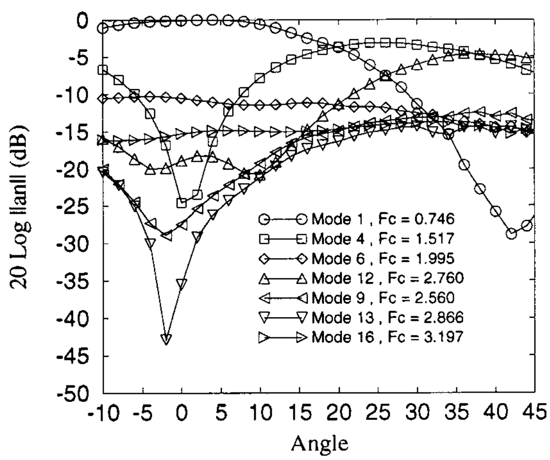

Fig. 7. "CHANNEL," $\phi\phi$ polarization, $F = 4$ GHz modal decomposition on the fictitious surface Γ_1.

rior domain V_0 leads to 64 470 surface unknowns and the scattering matrix S_0 is computed with the EFIE solver. The interior inlet domain has been evaluated first with the EFIE with one volume (59 016 surface unknowns), and secondly with 20 subdomains computed with the FEM method. The total number of volume unknowns processed with the FEM is 882 465. The tangent fields on Γ_1 were expanded with 24 propagating modes. The modal decomposition of the total electromagnetic field on Γ_1 is obtained through equation (15) and is plotted on the Figs. 7 and 8 for all the incidence angles. These coefficients are very useful for understanding the coupling phenomena and analyzing the field propagation in the air intake. The Figs. 9 and 10 show the RCS versus the angle of incidence in the $\phi\phi$ and $\theta\theta$ polarizations, the agreement with the measures is again very good.

B. Air Intake-Engine Geometry: "CHANNEL 16 Blades"

The geometry of this case is an evolutive inlet engine enclosed in a circular cylinder. The entry of the channel has an elliptic section, the end of the channel has a circular section, which is the fictitious surface between the end of the channel and a volume containing a 16 blades rotating structure. The object is perfectly conducting. The geometry is defined by the Figs. 11(a) and (b) and 12. The wave vector of the incident wave is directed along

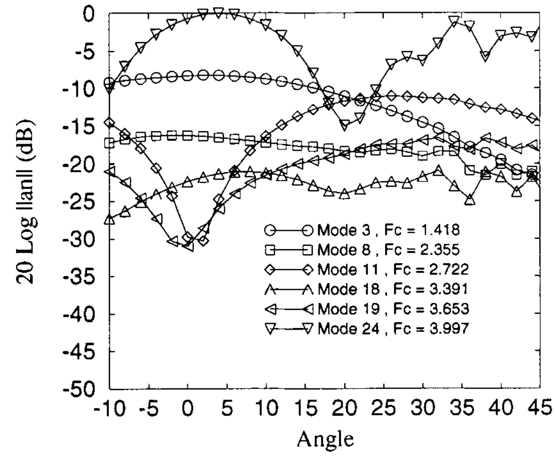

Fig. 8. "CHANNEL," $\theta\theta$ polarization, $F = 4$ GHz modal decomposition on the fictitious surface Γ_1.

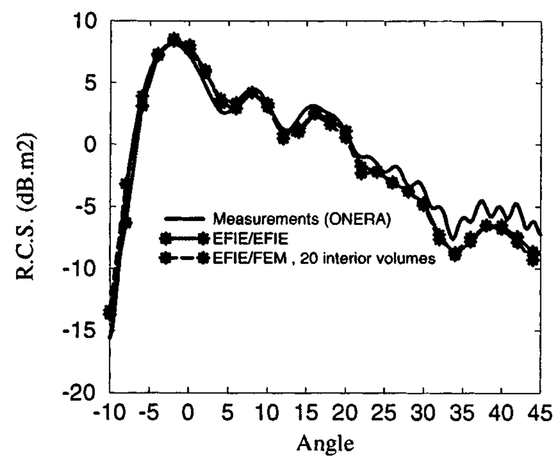

Fig. 9. Comparison of measured and computed near-field RCS for the air intake, $\theta\theta$ polarization, and $F = 4$ GHz.

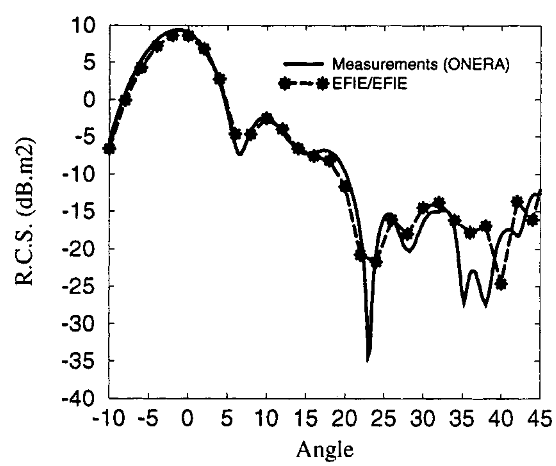

Fig. 10. Comparison of measured and computed near-field RCS for the air intake, $\phi\phi$ polarization, and $F = 4$ GHz.

$-X$, and the electric field is parallel to Y ($\phi\phi$ polarization) or to Z ($\theta\theta$ polarization). We have introduced a spherical incident wave generated at 8.355 m from the point (0.642, 0, 0) so as to reproduce the measurement conditions. The target is split into three volumes. V_0 is the exterior domain (25 806 unknowns),

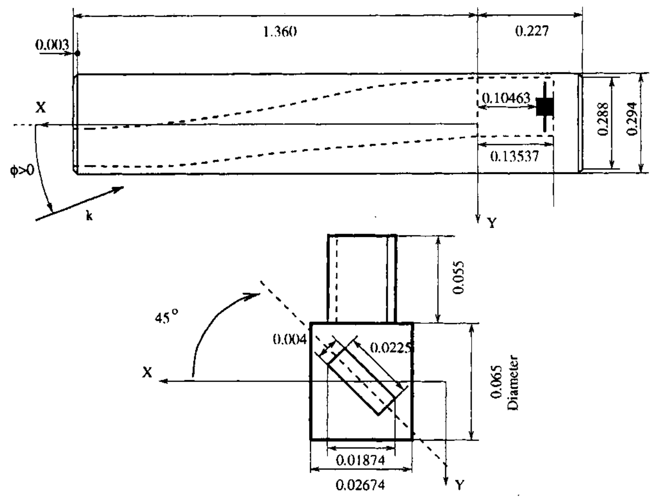

Fig. 11. (a) Geometry of the air-intake problem (all dimensions are in meters). (b) Geometry of the engine (only two blades of the 16 are shown).

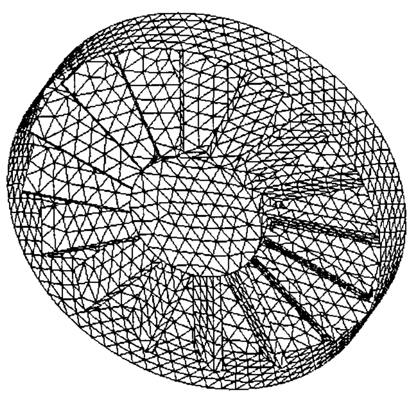

Fig. 12. Mesh of the engine volume V_2.

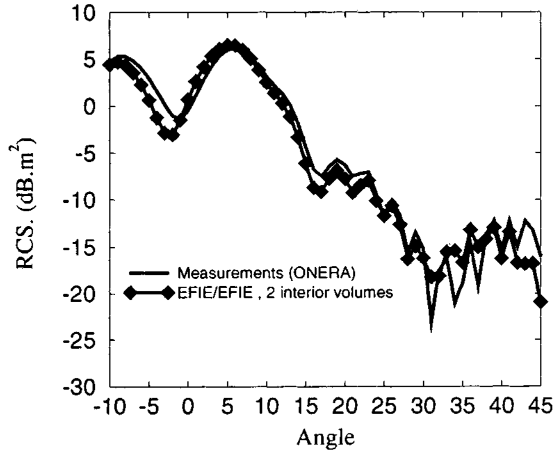

Fig. 13. Comparison of measured and computed far-field RCS for the air inlet engine, $\phi\phi$ polarization, and $F = 3$ GHz.

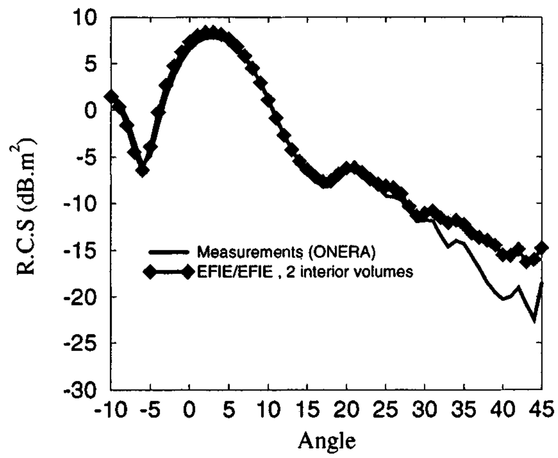

Fig. 14. Comparison of measured and computed far-field RCS for the air inlet engine, $\theta\theta$ polarization, and $F = 3$ GHz.

V_1 is the channel (26 850 unknowns) and V_2 the engine volume (6564 unknowns). All of them are computed with the EFIE. The tangent fields on Γ_1 are expanded with 13 propagating modes on Γ_1 and 17 on the circular surface Γ_2 between V_1 and V_2. Figs. 13 and 14 show the RCS versus the angle of incidence in the $\phi\phi$ and $\theta\theta$ polarizations. The results are in agreement with the measurements.

C. Antenna Geometry: "DENEB"

The geometry of this case is a rectangular horn enclosed in a circular cylinder. The horn is fed by an electronic network. The object is perfectly conducting. The geometry is defined by Fig. 15.

The frequency of interest is 4.5 GHz. The spherical incident wave is generated at 8.71 m from the point (0, 0, 0.251) (Appendix B). The mesh of V_0 leads to 32 904 surface unknowns and the scattering matrix S_0 is computed with the EFIE formulation. The interior horn domain V_1 has also been computed with the EFIE solver (7161 surface unknowns). The fictitious surface Γ_1 between V_0 and V_1 is located at 0.033 33 m from the aperture. The tangent fields on Γ_1 are expanded with 30 propagating modes. The vertical fundamental mode (electric field parallel to Y) is used on the second fictitious surface Γ_2 localized in the rectangular waveguide V_2 at 0.033 33 m from the junction with the rectangular horn. The scattering matrix S_2 of V_2 is measured for 23 states of the electronic network. These parameters are defined on the reference plane localized at the junction between the horn and the rectangular waveguide, i.e., at 0.0763 m from the termination of the cavity.

Fig. 16 shows the comparison between the computed and measured RCS versus the varying parameters of the electronic alimentation for an incidence angle of zero degree in the $\theta\theta$ polarization. The results are in agreement with the measurements.

IV. Efficiency

We shall now evaluate the computational savings of this method applied to 3-D inlet-engine domains. In this particular application, the cavity has one dimension much larger than the other two. In this evaluation, we suppose that each domain is computed with a standard integral equation and that the dense linear system is factorized with a direct solver.

The total computational time is the sum of the time for the matrix generation, factorization, and solution phases. If the mesh leads to n_{edges} unknowns, the computation time T_0 for n_{incid} incident waves is: $T_0 = (C_1/2)n_{\text{edges}}^2 + (4C_2/3)n_{\text{edges}}^3 + 8C_3 n_{\text{incid}} n_{\text{edges}}^2$.

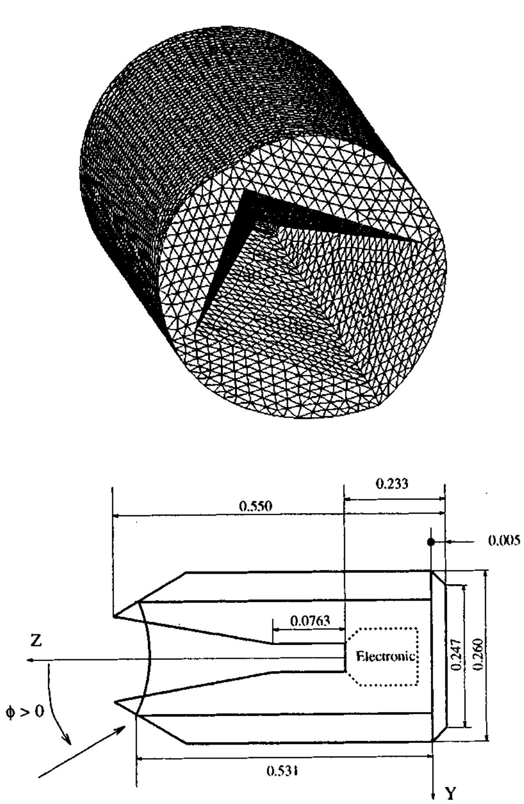

Fig. 15. Geometry of the DENEB problem (all dimensions are in meters).

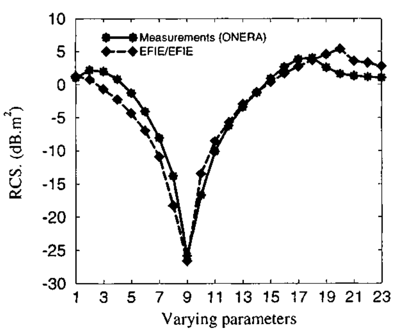

Fig. 16. Comparison of measured and computed modulated RCS for DENEB, Incidence zero degree, $\theta\theta$ polarization, and $F = 4.5$ GHz.

Suppose that the inlet is decomposed in P interior volumes each one possessing n_{modes} eigenmodes and n_f unknowns per fictitious surface. If the inlet is a circular cylinder of length L and radius R, we have $n_f \simeq (3/2)(\pi R^2/\sigma)$ with $\sigma = (\sqrt{3}/4)(\lambda/7)^2$, and $n_{\mathrm{modes}} \simeq \pi(2R/\lambda)^2 + (4R/\lambda)$. The total CPU required is approximately

$$T_P \simeq P\left\{\frac{C_1}{2}\,\frac{n_{\mathrm{edges}}^2}{P^2} + \frac{C_4}{2}\,\frac{n_{\mathrm{edges}} n_f}{P}\right\} + P\left\{\frac{4C_2}{3}\,\frac{n_{\mathrm{edges}}^3}{P^3}\right\} + P\left\{8C_3(n_{\mathrm{incid}} + n_{\mathrm{modes}})\frac{n_{\mathrm{edges}}^2}{P^2}\right\}. \qquad (18)$$

The coefficients C_1, C_2, C_3 and C_4 depend on the computer and linear solvers used. Fig. 17 shows the evolution of the speedup T_0/T_P as a function of the number of internal volumes for different frequencies and with the following coefficients obtained on ONERA's NEC SX-4 supercomputer: $C_1 = 1.1641\ 10^{-9}$ h, $C_2 = 1.4837\ 10^{-13}$ h, $C_3 = 1.5924\ 10^{-13}$ h, $C_4 = 5.6393\ 10^{-9}$ h. The length and the radius of the circular cylinder are $L = 1.363$ m and $R = 0.9235$ m, respectively. By using waveguide modes on the fictitious surfaces, the number of right-hand sides in (6) is n_{modes} and is smaller than the fictitious surface number of unknowns n_f as in [7], [6].

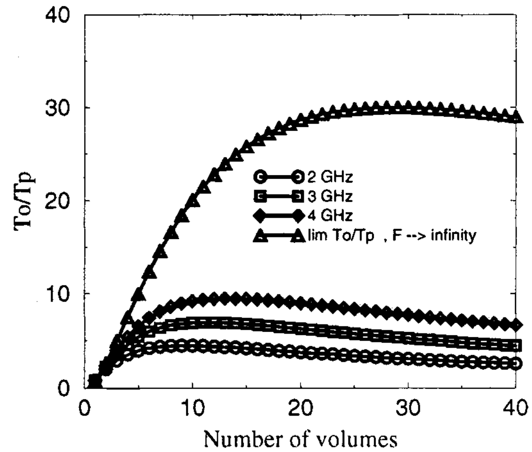

Fig. 17. Speedup of the method for inlet-engine domains.

In a context of parametric investigations where we need the global RCS of the target for K modifications in a volume V_i, the scattering matrices of the modified domains has to be re-evaluated, the other ones are only re-used before starting the connection step. We took advantage of this feature for all the validations proposed in this paper. Indeed, the exterior domain V_0 of "CHANNEL" has been computed with the EFIE and characterized by the scattering matrix S_0 only once and reused with each of the matrices S_{Int} obtained with different techniques (one EFIE domain at 2, 3, and 4 GHz, one FEM domain at 2 GHz, five EFIE domains at 2 GHz and 20 FEM domains at 4 GHz). In the "DENEB" antenna application, the exterior domain V_0 and the interior horn domain V_1 have been computed once and plugged into the connection scheme with the 23 measured scattering matrices of V_2. This plug and play algorithm is very efficient when using our waveguide modal expansion on the fictitious surfaces and leads to linear systems of small size both for assembling the inlet volumes and for coupling the exterior and the interior (15).

V. Conclusion

In this paper, we have introduced a multidomain and multimethod technique for analyzing the electromagnetic scattering from 3-D cavities. The FEM and the EFIE are used to compute the generalized Scattering matrices of the subdomains. We have used waveguide modes for modeling the field propagation from the cavity opening down to the obstacles or the engine face. RCS patterns of various complex cavities were presented and compared to measurements to show the accuracy of this method, the reduction in computation time and the advantage of this method for parametric studies.

APPENDIX A
CONNECTION ALGORITHM

Consider two inlet-engine adjacent volumes V_1 and V_2 of the global decomposition (Fig. 1). The number of interfaces between these volumes is one or two. They are characterized by the scattering matrices $[S_1]$ and $[S_2]$

$$\begin{pmatrix} b_1^1 \\ b_1^2 \end{pmatrix} = \begin{bmatrix} S_1^{11} & S_1^{12} \\ S_1^{21} & S_1^{22} \end{bmatrix} \cdot \begin{pmatrix} a_1^1 \\ a_1^2 \end{pmatrix}$$

$$\begin{pmatrix} b_2^1 \\ b_2^2 \end{pmatrix} = \begin{bmatrix} S_2^{11} & S_2^{12} \\ S_2^{21} & S_2^{22} \end{bmatrix} \cdot \begin{pmatrix} a_2^1 \\ a_2^2 \end{pmatrix}.$$

The connection algorithm consists in eliminating the coefficients associated to the common fictitious surface. A new volume is then generated and its scattering matrix is obtained from the blocks of $[S_1]$ and $[S_2]$

$$S^{11} = S_1^{12}.(I - S_2^{11}.S_1^{22})^{-1}.S_2^{11}.S_1^{21} + S_1^{11} \tag{19}$$

$$S^{12} = S_1^{12}.(I - S_2^{11}.S_1^{22})^{-1}.S_2^{12} \tag{20}$$

$$S^{21} = S_2^{21}.(I - S_1^{22}.S_2^{11})^{-1}.S_1^{21} \tag{21}$$

$$S^{22} = S_2^{21}.(I - S_1^{22}.S_2^{11})^{-1}.S_1^{22}.S_2^{12} + S_2^{22}. \tag{22}$$

APPENDIX B
MEASUREMENT CONDITIONS (ALL DIMENSIONS ARE IN METERS)

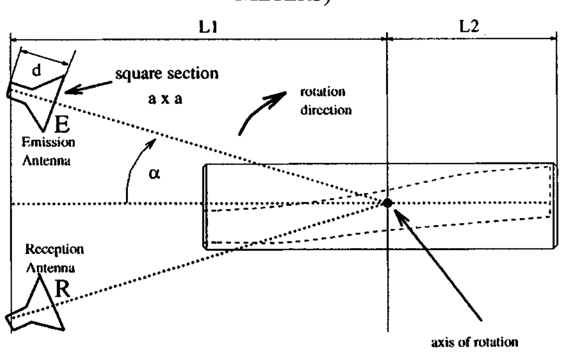

ACKNOWLEDGMENT

The authors would like to thank J. P. Marcellin and A. Cheraly for the definition of the CHANNEL target and the RCS measurements. They would also like to thank P. Dreuillet for the characterization of the DENEB antenna.

REFERENCES

[1] P. H. Pathak and R. J. Burkholder, "Modal, ray, and beam techniques for analyzing the EM scattering by open-ended waveguide cavities," *IEEE Trans. Antennas Propagat.*, vol. 37, pp. 635–647, May 1989.

[2] P. R. Rousseau and R. J. Burkholder, "A hybrid approach for calculating the scattering from obstacles within large open cavities," *IEEE Trans. Antennas Propagat.*, vol. 43, pp. 1068–1075, Oct. 1995.

[3] T. T. Chia, J. Burkholder, and R. Lee, "The application of FDTD in hybrid methods for cavity scattering analysis," *IEEE Trans. Antennas Propagat.*, vol. 43, pp. 1082–1090, Oct. 1995.

[4] D. C. Ross, J. L. Volakis, and H. Hannastassiu, "Hybrid finite element-modal analysis of jet engine inlet scattering," *IEEE Trans. Antennas Propagat.*, vol. 43, pp. 277–285, Mar. 1995.

[5] X. Yuan, D. R. Lynch, and J. W. Strohbehn, "Coupling of finite element and moment methods for electromagnetic scattering from inhomogeneous objects," *IEEE Trans. Antennas Propagat.*, vol. 38, pp. 386–391, Mar. 1990.

[6] J. C. Cheng, N. I. Dib, and L. P. B. Kathei, "Theoretical modeling of cavity-backed patch antenas using a hybrid technique," *IEEE Trans. Antennas Propagat.*, vol. 43, pp. 1003–1013, Sept. 1995.

[7] T. M. Wang and H. Ling, "Electromagnetic scattering from three-dimensional cavities via a connection scheme," *IEEE Trans. Antennas Propagat.*, vol. 39, pp. 1505–1513, Oct. 1991.

[8] J. M. Jin and J. L. Volakis, "A finite element-boundary integral formulation for scattering by three-dimensional cavity-backed apertures," *IEEE Trans. Antennas Propagat.*, vol. 39, pp. 97–104, Jan. 1991.

[9] J. J. Angélini, C. Soize, and P. Soudais, "Hybrid numerical method for harmonic 3-D Maxwell equations: scattering by a mixed conducting and inhomogeneous anisotropic dielectric medium," *IEEE Trans. Antennas Propagat.*, vol. 41, pp. 66–76, Jan. 1993.

[10] P. Soudais, "Computation of the electromagnetic scattering from complex 3D objects by a hybrid FEM/BEM method," *J. Electromagn. Waves Applicat.*, vol. 9, pp. 871–886, July 1995.

[11] P. Soudais, H. Stève, and F. Dubois, "Scattering from several test-objects computed by 3D hybrid IE/PDE methods," *IEEE Trans. Antennas Propagat.*, vol. 47, pp. 646–653, Apr. 1999.

[12] P. P. Silvester and R. L. Ferrari, *Finite Elements for Electrical Engineers*, 2 ed. Cambridge, MA: Cambrige Univ. Press, 1990.

[13] A. Barka, A. Cosnuau, and F. X. Roux, "Parallel organization of air intake electromagnetic mode computation on a distributed memory machine," *La Recherche Aérospatiale*, no. 6, 1995.

[14] S. M. Rao, D. R. Wilton, and A. W. Glisson, "Electromagnetic scattering by surfaces of any shape," *IEEE Trans. Antennas Propagat.*, vol. AP-30, pp. 409–418, May 1982.

[15] J. C. Nedelec, "Mixed finite elements in R^3," *Numerische Mathematik*, vol. 35, pp. 315–341, 1980.

[16] G. L. James, "Analysis and design of TE_{11} to HE_{11} corrugated cylindrical waveguide mode convectors," *IEEE Trans. Microwave Theory Tech.*, vol. MTT-29, Oct. 1981.

André Barka was born in Périgueux, France, in 1963. He received the M.S. and Ph.D. degrees in applied mathematics from the University of Bordeaux, France, in 1986 and 1990, respectively.

Since 1989, he has been working as a Research Engineer at ONERA in the System Department and then in the Electromagnetism and Radar Department. His current research deals with finite-element methods, hybrid methods, and electromagnetics.

Paul Soudais was born in Paris, France, in 1965. He received the Diplôme d'Ing. and Ph.D. degree from the Ecole Centrale de Paris, France, in 1988 and 1995, respectively.

Since 1989, he has been working as a Researcher at ONERA in the Structures Department and then in the Electromagnetism and Radar Department. In 1994 he participated in a U.S.–French Scientist and Engineer Exchange Program as a Visiting Researcher in the Department of Electrical Engineering and Computer Science, University of Illinois at Chicago.

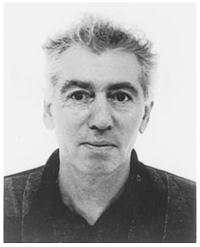

Dominique Volpert was born in Tunis, Tunisie, in 1942. He received the Diplôme d'Ing. degree from the Ecole Superieure de l'Aeronautique et de l'Espace, France, in 1966, and the M.S. degree in mathematics from the Universite of Paris, France, in 1967.

From 1967 to 1970, he worked at Avions Marcel Dassault, Paris, France. Since 1971 he has been a Research Engineer with ONERA, first in the Automatic Department and then in the Numerical Analysis Department. His current research deals with partial derivative equation and finite elements. He is also a Professor of applied mathematics at the Ecole Superieure de l'Aeronautique et de l'Espace, Toulouse, France.